MEASUREMENT OF ANGULAR AND MOMENTUM DISTRIBUTIONS OF CHARGED PARTICLES WITHIN AND AROUND JETS IN Pb+Pb AND *pp* COLLISIONS AT $\sqrt{S_{\mathrm{NN}}} = 5.02$ TeV WITH ATLAS AT THE LHC

BY

AKSHAT PURI

DISSERTATION

Submitted in partial fulfillment of the requirements
for the degree of Doctor of Philosophy in Physics
in the Graduate College of the
University of Illinois at Urbana-Champaign, 2019

Urbana, Illinois

Doctoral Committee:

Professor Matthias Grosse Perdekamp, Chair
Professor Anne Marie Sickles, Advisor
Professor Aida El-Khadra
Professor Bryce Gadaway

Abstract

Studies of the fragmentation of jets into charged particles in heavy-ion collisions can help in understanding the mechanism of jet quenching by the hot and dense matter created in such collisions, the quark-gluon plasma. This thesis presents a measurement of the angular distribution of charged particles around the jet axis as measured in Pb+Pb and *pp* collisions collided at a center of mass energy of $\sqrt{s_{\mathrm{NN}}} = 5.02$ TeV. The measurement is done using the ATLAS detector at the Large Hadron Collider, and utilizes 0.49 pb^{-1} of Pb+Pb and 25 pb^{-1} of *pp* data collected in 2015. The measurement is performed inside jets reconstructed with the anti-k_t algorithm with radius parameter $R = 0.4$, and is extended to regions outside the jet cone. Results are presented as a function of Pb+Pb collision centrality, and both jet and charged-particle transverse momenta. It was observed that in Pb+Pb collisions there is a broadening of the jet for charged particles with $p_{\mathrm{T}} < 4$ GeV, along with a narrowing for charged particles with $p_{\mathrm{T}} > 4$ GeV. Ratios between the angular distributions in Pb+Pb and *pp* showed an enhancement for particles with $p_{\mathrm{T}} < 4$ GeV in Pb+Pb collisions, with the enhancement increasing up to 2 for $r < 0.3$, and remaining constant for $0.3 < r < 0.6$. Charged particles with $p_{\mathrm{T}} > 4$ GeVshow a growing suppression of up to 0.5 for $r < 0.3$ in Pb+Pb collisions, with the depletion remaining constant for $0.3 < r < 0.6$.

For my Mother, Father, and Brother

Chapter 1

Introduction

The Large Hadron Collider (LHC) at the European Center for Nuclear Research (CERN), is one of the worlds most expensive and complicated machines, and was built with the purpose of accelerating subatomic particles to close to the speed of light and colliding them to study their underlying structure. Detectors around the LHC ring, the biggest of which are ATLAS (A Toroidal LHC ApparatuS), CMS (Compact Muon Solenoid), ALICE (A Large Ion-Collider Experiment), and LHCb (LHC-Beauty), study these collisions and use the debris as a playground to verify and expand the "Standard Model" of particle physics. This thesis will focus on measurements of collisions involving heavy ions, as measured by the ATLAS detector.

Relativistic heavy ion collisions such as those at the LHC provide insight into the interactions between quarks and gluons. These fundamental building blocks of all matter interact via the strong force, the theoretical framework of which is described by Quantum Chromodynamics (QCD). This theory dictates that quarks and gluons are confined, i.e. locked together to form composite particles and cannot exist independently, making their study extremely difficult. Relativistic heavy ion collisions provide an extreme environment where nuclear matter can "melt" and form a deconfined medium that consists of free quarks and gluons. This state of matter, called the Quark Gluon Plasma (QGP) is what existed a few microseconds after the Big Bang, and is what eventually cooled and expanded to form the existing universe.

The quark-gluon plasma (see Refs. [1, 2] for recent reviews) can be probed by jets, sprays of particles that come from hard scattering processes between the nucleons involved in the collision. These jets are produced early in the collision, and interact with the QGP as they make their way to the detector. Studying the rates and characteristics of these jets in Pb+Pb collisions, and comparing them to similar quantities in *pp* collisions can provide information on the properties of the QGP.

This thesis is split into 4 main chapters. An overview of the LHC and the ATLAS detector is given in Chapter **??**, Chapter **??** will describe the QCD framework that will give context to the measurements discussed, Chapter **??** will describe the work undertaken to become a member of the ATLAS Collaboration, and Chapter **??** will provide a detailed description of the measurement to determine the angular distributions of charged particles in Pb+Pb and *pp* collisions.

Chapter 2

Experimental Setup

2.1 The Large Hadron Collider

The Large Hadron Collider (LHC) is part of the European Organization for Nuclear Research. It has a circumference of 27 kilometers, making it the world's largest particle accelerator, and is housed in a tunnel that is up to 175 meters below the surface of the earth. The LHC has eight arcs and eight straight sections, with each straight section being approximately 528 m long. The arc sections are built using 1232 dipole superconducting magnets, providing a magnetic field of up to 8.33 T. Another 392 quadrupole magnets are used for focussing the beam. The magnets are cooled down to 1.9 K via liquid Helium. The LHC beam pipe has two rings with counter-rotating beams and uses a uses a twin-bore magnet design that optimizes for both cost, as well as space. The counterrotating beams require opposite magnetic dipole fields in both rings, with separate magnetic and vacuum chambers, with the common sections only at the insertion regions, where the major experimental detectors are located. These detectors are: A Toroidal LHC Apparatus (ATLAS), Compact Muon Solenoid (CMS), A Large Ion Collider Experiment (ALICE), and Large Hadron Collider - Beauty (LHCb) [**Evans:2008zzb**].

Capable of reaching up to center of mass energies, $\sqrt{s} = 14$ TeV for protons and $\sqrt{s_{NN}} = 5.5$ TeV for lead ions, the LHC delivers up to $10^{34}\text{cm}^2\text{s}^1$ of luminosity to the ATLAS and CMS detectors when colliding protons. The LHCb detector is a lower luminosity experiment, that receives up to $10^{32}\text{cm}^2\text{s}^1$, and ALICE, a dedicated ion experiment aims at a peak luminosity of $10^{27}\text{cm}^2\text{s}^1$ for nominal lead-lead operation. The beams in the LHC are accelerated by 16 radio frequency (RF) cavities that provide a voltage of 2 MV and operate at 400 MHz. They consist of bunches of protons or ions that are kept in their circular path by the dipole magnets, and focussed via the quadrupole magnets,

A schematic of the entire accelerator complex and the path followed by protons and heavy ions is show in Fig. **??**. Protons are obtained by stripping the hydrogen atom of its electrons via an electric field. The complete ionization of lead is done in multiple stages, with the first stage providing for Pb^{+29} via an ion source. Both the protons and heavy ions are then are accelerated by increasingly powerful accelerators, until

they reach the main LHC beam pipes. Protons start at LINAC 2 (LINear ACcelerator), whereas the lead ions start at LINAC 3. The Pb^{+29} lead ions are further stripped of electrons by passing them through a 0.3 μm foil after the LINAC 3. The Pb^{+54} ions are selected via mass spectrometer and sent to the Low Energy Ion Ring (LEIR), whereas the protons are sent to the Booster. They are then sent to the Proton Synchrotron (PS), followed by the Super Proton Synchrotron (SPS), and then finally the LHC. The final stripping of lead ions takes place after the PS, on a 0.8 mm thin aluminum foil.

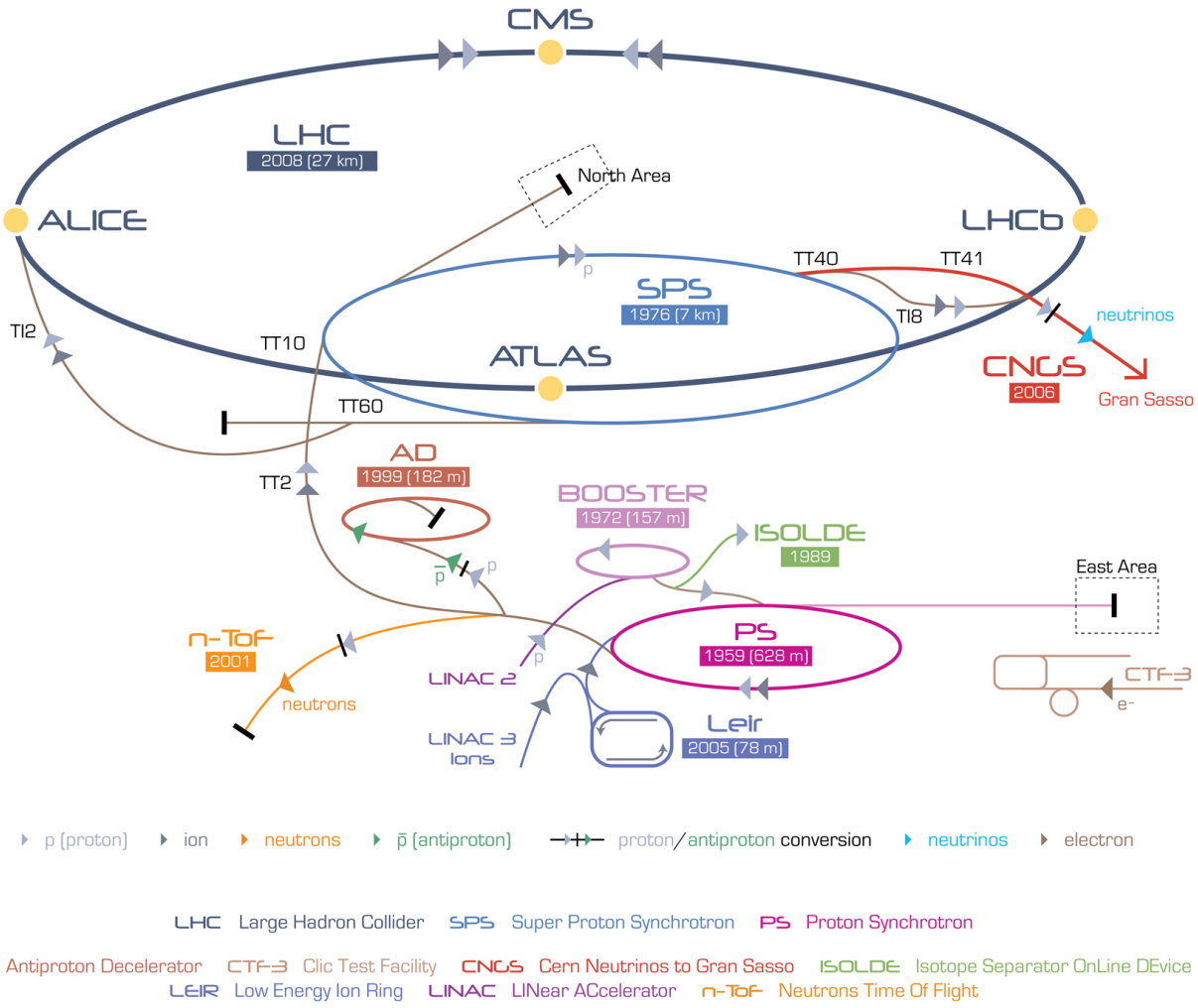

Figure 2.1: The accelerator complex at CERN. ATLAS can be seen inside the SPS on the LHC ring. Figure taken from Ref. [**TEEPCLPC**]

2.2 The ATLAS Detector

The ATLAS detector (Fig. **??**) is a general purpose detector at the LHC. It uses a right-handed coordinate system with its origin at the nominal interaction point (IP) in the centre of the detector and the z-axis along

the beam pipe. The x-axis points from the IP to the centre of the LHC ring, and the y axis points upward. Cylindrical coordinates (r, ϕ) are used in the transverse plane, ϕ being the azimuthal angle around the beam pipe. The pseudorapidity is defined in terms of the polar angle θ as $\eta = -\ln\tan(\theta/2)$.

The detector was designed keeping in mind the goals of the physics it aimed to explore, and as such has the following characteristics:

- dsf
- dsf
- dsf

The detector is symmetric in the forward-backward direction, and has a full 2π coverage in azimuth

The A side of the detector is defined as having positive z, withe C side being defined as having negative z.

It has three main subsystems: the inner detector, the calorimeter, and the muon spectrometer. This paper will only discuss the inner detector and the calorimeter, since those are the systems that will be used in the analysis.

ATLAS uses a

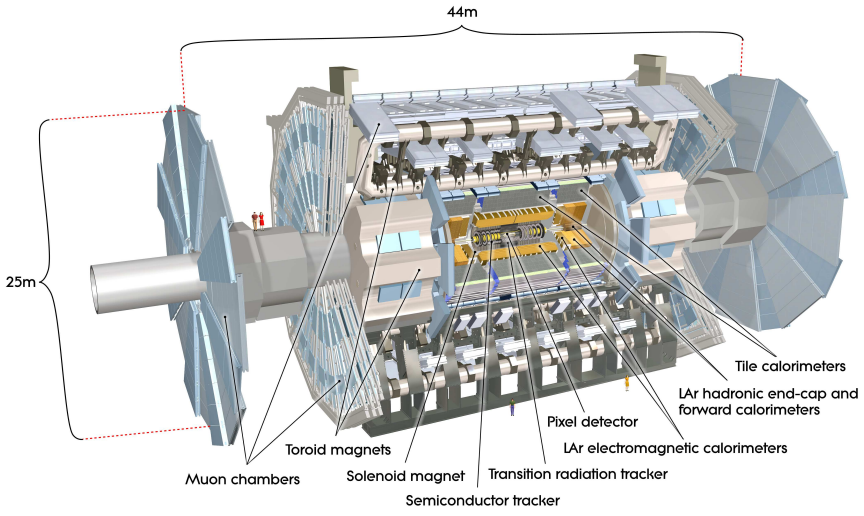

Figure 2.2: The ATLAS detector. Figure taken from Ref. [3].

Inner Detector

The inner detector (Fig. **??**) is designed to reconstruct the charged particle trajectories in the interval $|\eta| < 2.5$. This is achieved by a combination of three subsystems: the Pixel detector, the Semiconductor

Tracker (SCT), and the straw-tube Transition Radiation Tracker (TRT), all immersed in a 2T magnetic field [3].

The pixel detector consists of four layers of pixels, with the innermost layer at a distance of 33.25 mm from the interaction point. The expected hit resolution of the pixel detector ranges from of $\sim 8\mu$m ($\sim 40\mu$m) in $r-\phi$ (z) [**ibl˙design**] for the innermost layer, to $\sim 10\mu$m ($\sim 115\mu$m) in $r-\phi$ (z) for the next three layers [3].

The SCT has eight strip (80 μm pitch) layers that are crossed by each track. Small angle stereo strips are used to measure both coordinates, with one set of strips in each layer, parallel to the beam direction. The end cap region has nine layers of double sided modules with strips in the radial direction, with each also having a mean pitch of 80 μm. The intrinsic resolution is $\sim 17\mu$m ($\sim 580\mu$m) in $r-\phi$ (z) [3].

The TRT contains 73 (160) layers of straws and fibers in the barrel (end-cap), and provides a large number of hits per track, allowing track-following for $|\eta| < 2.0$. T. It has a resolution of $\sim 130\mu$m in $r-\phi$, with no information in the z direction [3].

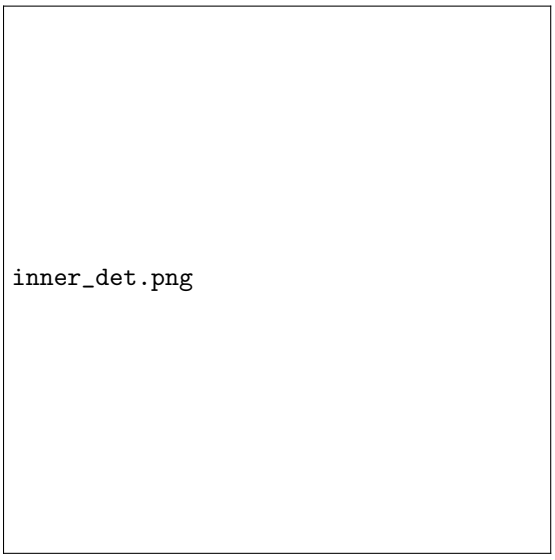

(a) ATLAS Inner Detector System

(b) A cut-away view of the ATLAS calorimeter system. Taken from [3]

Figure 2.3: ATLAS Inner detector and calorimeter systems

Calorimeter

The calorimeter system (Fig. **??**) covers the region $|\eta| < 4.9$, using different techniques over different ranges.

The sampling liquid argon (LAr) electromagnetic calorimeter (EMCal) covers $|\eta| < 3.2$ (the barrel region

for $|\eta| < 1.475$ and two end caps for $1.375 < |\eta| < 3.2$) . Its accordion-like geometry provides full ϕ symmetry without azimuthal cracks. The EMCal is segmented longitudinally into three layers, plus a presampler, with the granularity varying as a function of layer depth and pseudorapidity. The presampler ($|\eta| < 1.8$) compensates for the energy lost by photons and electrons upstream of the calorimeter [3].

The hadronic calorimeters (HCal) consist of the Tile, Hadronic End Cap (HEC), and the Forward Calorimeters (FCal). The Tile is placed directly outside the EMCal, covering $|\eta| < 1.0$, with the extended barrels covering the range $0.8 < |\eta| < 1.7$. It uses steel as the absorber and scintillating tiles as the active material. It has three layers, with the two sides of the tiles being read out by wavelength shifting fibers into separate photomultiplier tubes. The HEC consists of two wheels per cap, and is directly behind the EMCal end cap. It covers $1.5 < |\eta| < 3.2$, overlapping both the tile and the FCal (at $|\eta| = 3.1$). The active material in the HEC is LAr (with copper plates acting as the absorber). The FCal, ranging from $3.1 < |\eta| < 4.9$, consists of three modules in each end cap; the first, made of copper, is optimized for electromagnetic interactions, while the other two, made of tungsten, are optimized for hadronic measurements [3].

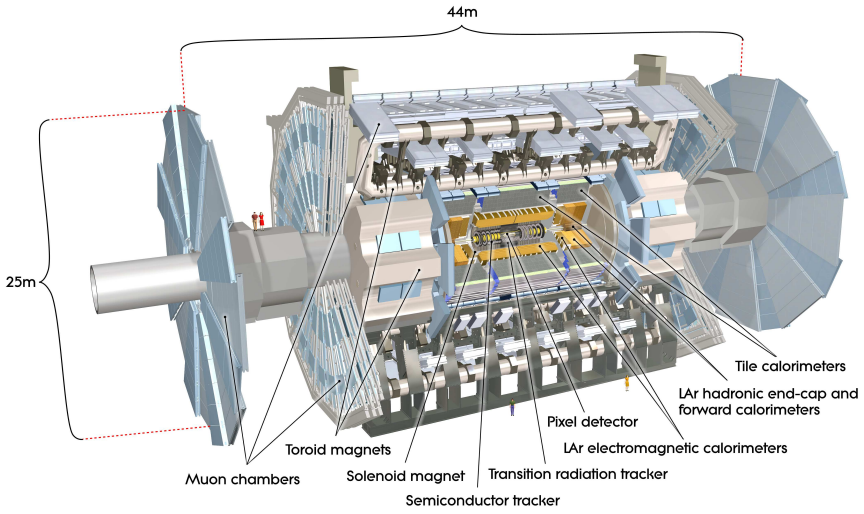

Figure 2.4: The ATLAS detector. Figure taken from Ref. [3].

The ATLAS detector [3], shown in Fig. **??** is one of the two larger detectors on the LHC and is located at interaction point 1 (IP1) on the LHC ring[1] It is designed to perform measurements of Standard Model physics, including the search for the Higgs boson, and search for physics beyond the Standard Model.

[1] ATLAS uses a right-handed coordinate system with its origin at the nominal interaction point (IP) in the centre of the detector and the z-axis along the beam pipe. The x-axis points from the IP to the centre of the LHC ring, and the y axis points upward. Cylindrical coordinates (r, ϕ) are used in the transverse plane, ϕ being the azimuthal angle around the beam pipe. The pseudorapidity is defined in terms of the polar angle θ as $\eta = -\ln\tan(\theta/2)$. Angular distance is measured in units of $\Delta R \equiv \sqrt{(\Delta\eta)^2 + (\Delta\phi)^2}$. Rapidity is defined in terms of energy and momentum of a particle or jet as $y = \frac{1}{2} ln(\frac{E+p_z}{E-p_z})$. The rapidity with center-of-mass frame boost accounted for is denoted $y^*_{\rm jet}$.

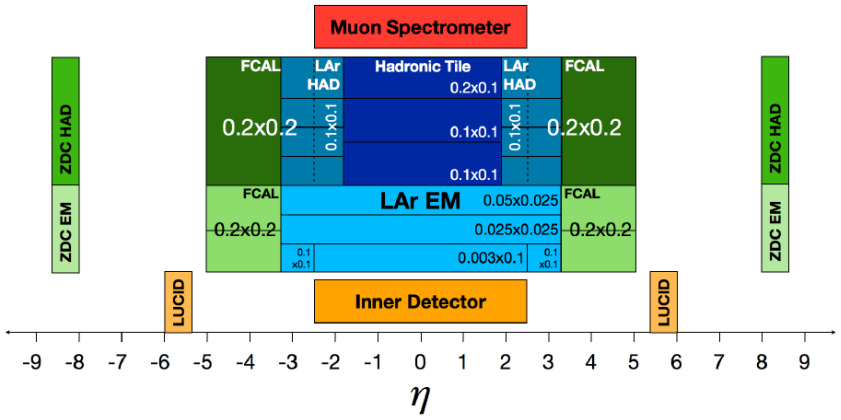

Figure 2.5: ATLAS detector pseudorapidity coverage. All components cover 2π in azimuth.

Although ATLAS is primarily a detector used to measure *pp* collisions, it has also been used to study Heavy Ion physics with much higher nuclear collision energies and much larger particle multiplicities compared to *pp* collision.

The ATLAS detector consists of four main parts, or sub-detectors. The closest part to the interaction point is the Inner Detector (ID), which is placed close to the IP and is used to measure charged particle tracks. The ID is inside a 2 Tesla solenoidal magnetic field, which causes charged particles to curve, allowing their momentum to be measured. Outside of the ID are the electromagnetic (EM) and hadronic calorimeters. These give energy measurements and are the primary detectors for the analysis presented in this thesis. The fourth and outermost part is the muon spectrometer which is placed inside a toroidal field provided by eight toroid magnets. The muon system is the outermost part of the detector because due to their weakly interacting nature, muons are one of the only particles which pass through the calorimeters. All of the ATLAS sub-detectors have full 2π azimuthal coverage and different pseudorapidity coverages shown in Fig. **??**. A detailed description of the ATLAS detector and it's subsystems can be found in [3].

2.2.1 ATLAS Trigger System

In order to select events during data-taking, a complex hardware and software system called the *trigger* is required. It relies on many detector subsystems to flag events based on a set of rules that are defined prior to each run. A two-level trigger system was used to select the *pp* and *p*+Pb collisions analyzed for the measurement presented in this thesis. The first, the hardware-based trigger stage Level-1 (L1), is implemented with custom electronics. The second level is the software-based High Level Trigger (HLT). The HLT consists of the Level-2 (L2) trigger, followed by the event filter (EF). The ATLAS trigger was designed for a collision rate of 40 MHz, with the L1 trigger designed to reduce the rate to 75 kHz, and the HLT

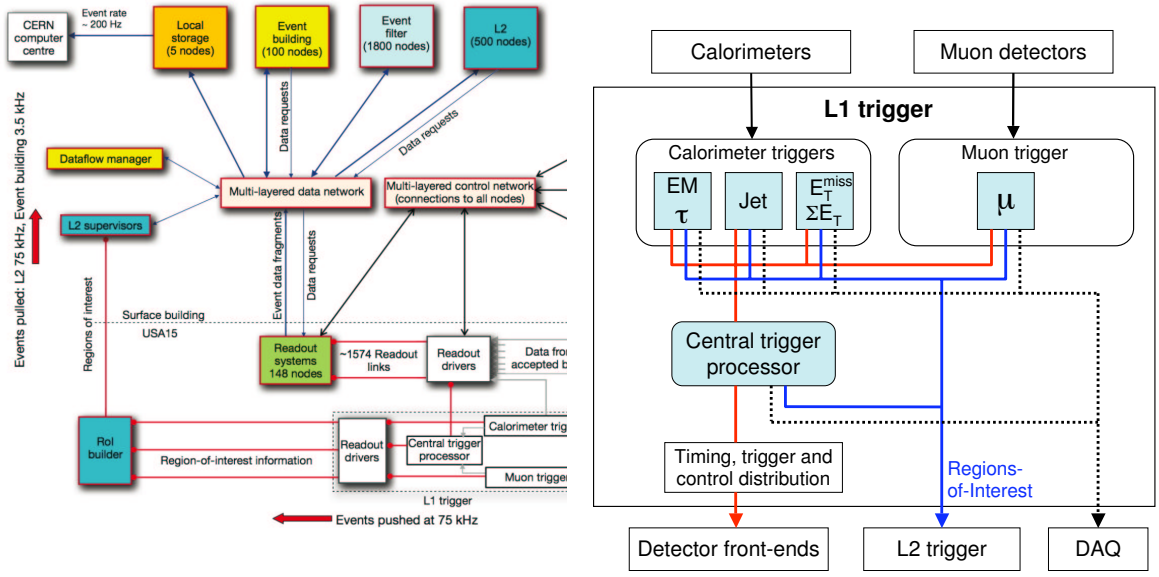

Figure 2.6: A schematic (left) of the ATLAS trigger and data acquisition systems, and the L1 hardware trigger (right). The total event rate of about 40 MHz is reduced by the L1 trigger to about 75 kHz, and further reduced to 200 Hz by the HLT (L2 + EF) trigger.Figure taken from Ref. [3].

to perform a final reduction to about 200 Hz, which is the final even rate written to disk. A schematic of the ATLAS trigger and data acquisition systems can be seen in Fig. **??**. Some triggers selecting minimum-bias (MB) events used the minimum-bias trigger scintillator detectors (MBTS). The MBTS detect charged particles over $2.1 < |\eta| < 3.9$ using two segmented counters placed at $z = \pm 3.6$ m. Each counter provides measurements of both the pulse heights and the arrival times of ionization energy deposits [3].

Some triggers can be prescaled, meaning that not every event meeting the requirements of a particular trigger is saved to disk. If a trigger with prescale c_p is saved n times, this corresponds to $c_p n$ events passing through the HLT. The decision of what prescale to assign to a trigger is very complicated. Various physics analysis groups have different requirements, but unfortunately not all data from a run can be saved due to technical limitations. Depending on the physics goals of a particular run, the trigger menu, which assigns the triggers and their respective prescales, will change. The UIUC ATLAS group has been responsible for the trigger system operation in all of the heavy ion runs since 2015.

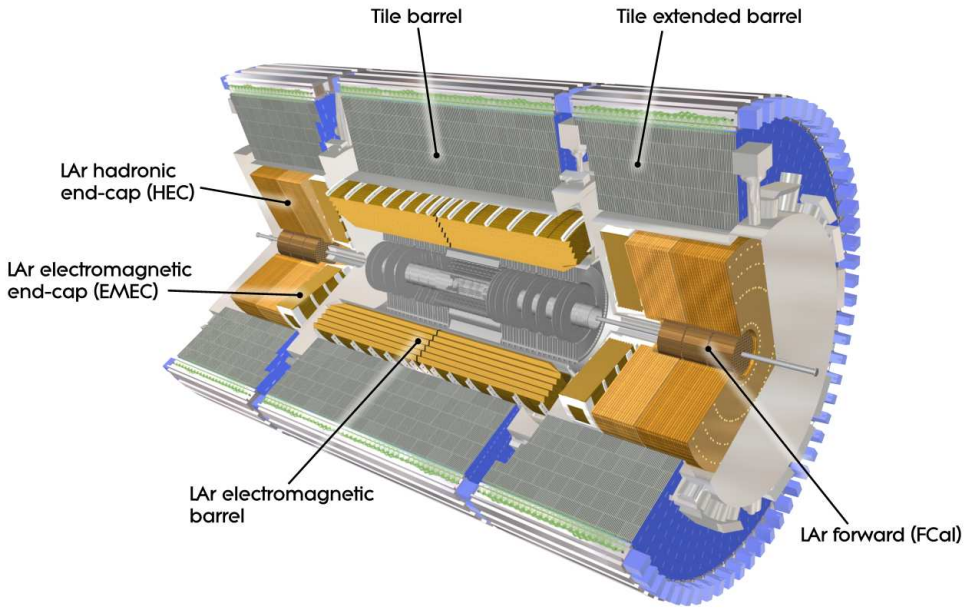

Figure 2.7: The ATLAS calorimeter system. Figure taken from Ref. [3].

2.2.2 Calorimetery

The ATLAS calorimeter system [3] is the main system used for the present analysis, a picture of this system is shown in Fig. **??**. The calorimeters are of sampling and non-compensating nature with a pseudorapidity coverage of $|\eta| < 4.9$. The non-compensating nature gives a different response on the EM and hadronic scales, and this is corrected in the calibration procedure. A sampling calorimeter is one where two distinctly different materials are chosen, one to produce a particle shower, and the other to measure the deposited energy.

There are two different sampling technologies used in the ATLAS calorimeter system. One technology is where liquid argon (LAr) is interspaced with lead, which acts as the absorber material. This is used in all of the ATLAS EM systems - the electromagnetic barrel (EMB), electromagnetic end-cap (EMEC), forward calorimeter (FCal), as well as the hadronic end-cap (HEC). Shower development starts in the absorber, and due to moving electrons and ions from ionization in the active material (LAr), a signal can be read out from induced charge on copper electrodes. The LAr gap is subject to a high voltage electric field in order to direct the ionized electrons and ions to the electrodes in a predictable way. The second technology, used in the hadronic tile calorimeters (TileCal), uses absorber material interspaced with plastic scintillator. The readout is different from the LAr case since scintillation light converted by wavelength shifting fibers and transported to photomultipliers instead of reading induced charge from ionization in LAr.

EM Calorimeters

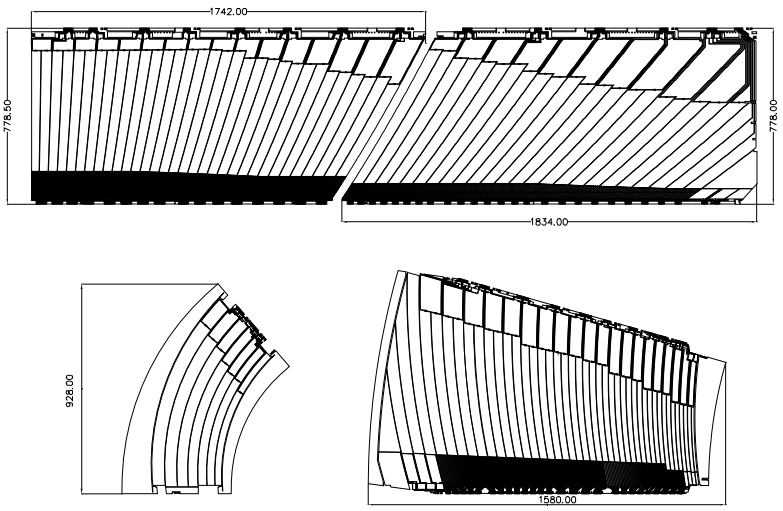

Figure 2.8: Layouts of a barrel EM module (top), inner end-cap wheel (bottom left), and outer end-cap wheel (bottom right). Figure taken from Ref. [3].

The ATLAS LAr electromagnetic calorimeter as chosen to have have an accordion geometry to minimize capacitance in the detecting elements. It is split into a barrel part covering $|\eta| < 1.475$, and two end-caps covering $1.375 < |\eta| < 3.2$. The accordion design allows modules to have multiple layers in depth, with varying granularity ($\Delta\eta \times \Delta\phi$). Layouts of segments from the barrel and end-cap EM calorimeters are shown in Fig. **??**. A detailed sketch of a barrel EM module and its constituent layers is shown in Fig. **??**. All components are placed into cryostats at a temperature of approximately 86° K [**Bremer:449276**]. The design and size of the EM calorimeter provides a total thickness of at least 22 radiation lengths (X_0). One X_0 represents the average distance an electron must travel through a material to reduce its energy to $1/e$ of its initial energy [**Fabjan:2003aq**]. The cumulative thickness of the calorimeter system can be seen as a function of pseudorapidity in Fig. **??**. All EM calorimeter systems were designed and tested to have an energy resolution of $\sigma(E_T)/E_T = 10\%/\sqrt{E_T} \bigoplus 0.7\%$.

A typical pulse in the LAr calorimeter originates from ionization electrons in the LAr gap. An electric field inside the gap collects the electrons and an ionization pulse is then read out and shaped. An ionization pulse is triangular in shape has a width of ∼450 ns [**Nikiforou:2013nba**], as can be seen in Fig. **??**. The final pulse that is digitized has a width between 450 and 600 ns after shaping. This corresponds to roughly 18 to 24 LHC bunch crossings. During this time, there could be contributions from out-of-time events (pile-up), and various techniques such as optimal filtering [**OliveiraDamazio:1630826**] have been developed to minimize contributions from pile-up.

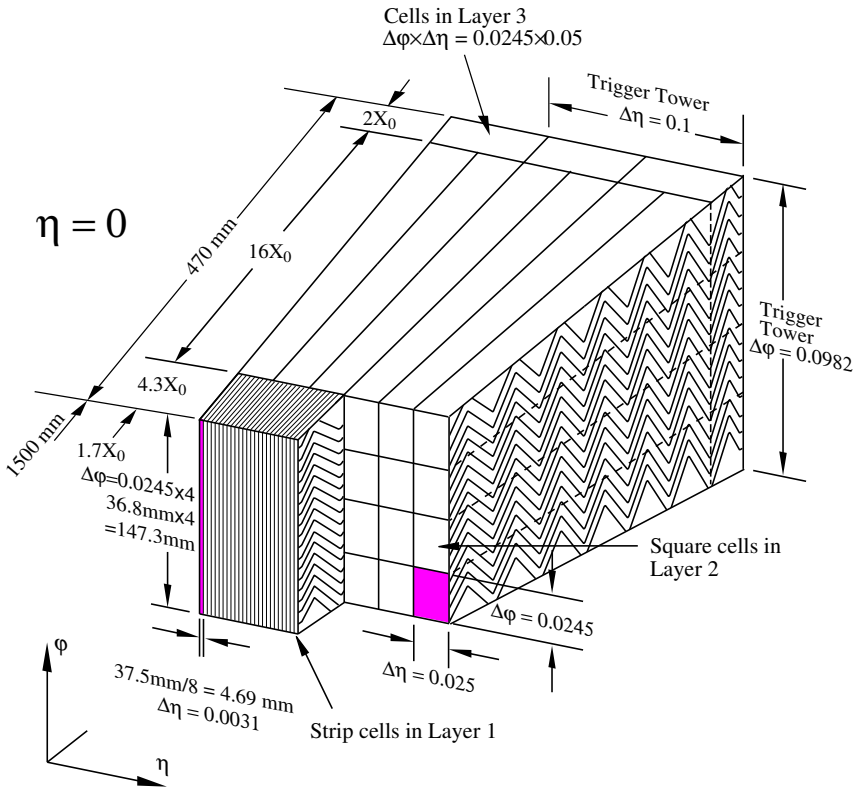

Figure 2.9: Sketch of a barrel EM module showing the different layers and their respective granularities. Radiation length (X_0) is the average distance an electron must travel through a given material to reduce its energy to $1/e$ of its initial energy. Trigger towers are sets of cells (strip or square) from which analog signals are summed for input to the L1 trigger. Figure taken from Ref. [3].

EM Barrel Calorimeter

The EM barrel, covering $|\eta| < 1.475$, consists of two half-barrels, each 3.2 meters long and weighing 57 tons. It has an inner and outer diameter of 2.8 m and 4.0 m, respectively. The calorimeter is comprised of three layers, with a thickness of at least 22 X_0 increasing to from 22 to 30 X_0 in the interval $0 < |\eta| < 0.8$, and from 24 to 33 X_0 in the interval $0.8 < |\eta| < 1.3$, as seen in Fig. **??**. In front of these three layers is a LAr presampler which is intended to recover energy lost to material in front of the EMCal. The granularity of the EM barrel calorimeter's first layer is $\Delta\eta \times \Delta\phi = 0.025 \times 0.025$ in order to be able to perform shower shape measurements and to distinguish pairs of γ from π^0 decays with pairs of γ from H decay. The granularity of the presampler is $\Delta\eta \times \Delta\phi = 0.025 \times 0.1$.

EM End-cap Calorimeter

The EM end-cap calorimeter, covering $1.375 < |\eta| < 3.2$, consists of two wheels on each side of the EM barrel calorimeter, each 63 cm thick, with a weight of 27 tons. Each wheel of the EM end-cap calorimeter consists

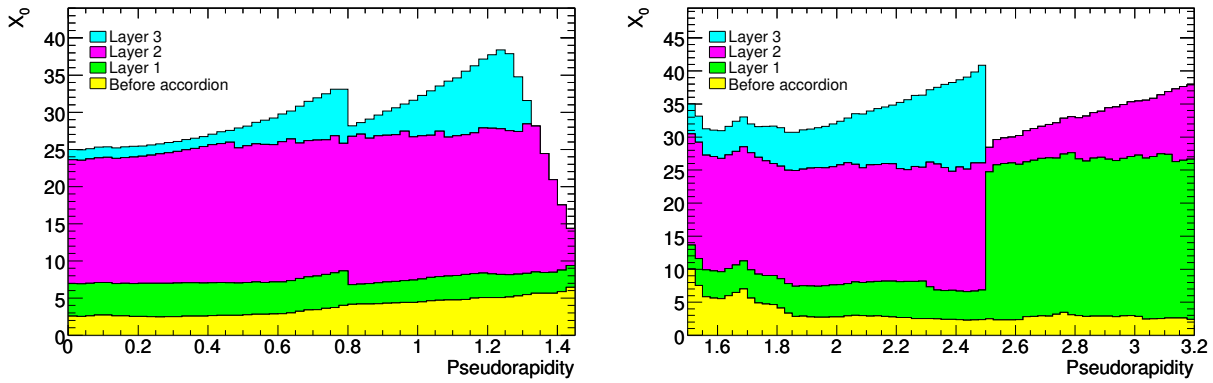

Figure 2.10: Cumulative thickness, in units of radiation length X_0 and as a function of $|\eta|$, in front of (yellow distribution) and in the electromagnetic calorimeters. Shown separately are the amounts of radiation in the various layers of the barrel (left) and end-cap (right) EM calorimeters. Figure taken from Ref. [3].

of 32 identical azimuthal sectors. Similar to the EM barrel calorimeter, the barrel end-cap calorimeter consists of three layers. It has a total thickness of at least 24 X_0 increasing from 24 to 38 X_0 on the outer wheel ($1.475 < |\eta| < 2.5$), and from 26 to 36 X_0 on the inner wheel ($2.5 < |\eta| < 3.2$). Similar to the EM barrel calorimeter, the granularity of the first layer is $\Delta\eta \times \Delta\phi = 0.025 \times 0.025$ and the granularity of the presampler is $\Delta\eta \times \Delta\phi = 0.025 \times 0.1$.

Hadronic Calorimeters

The hadronic calorimeters surround the EM calorimeters and are designed to measure the energy deposited from hadrons and hadronic showers that passed through the EM calorimeters. Characteristic distance for hadronic calorimeters is described by the nuclear interaction length λ_I, which is the hadronic equivalent to a radiation length. For the EM calorimeter system, λ_I is small, requiring hadronic calorimeters to have sufficiently larger thicknesses in order to fully contain hadronic showers. The hadronic calorimeter is composed of the Tile barrel calorimeter with a coverage $|\eta| < 0.8$, the Tile extended barrel with a coverage $0.8 < |\eta| < 1.7$, and the HEC with a coverage $1.5 < |\eta| < 3.2$. Both Tile systems use steel as an absorber, with scintillator as the active material. The particle shower begins in the absorber, and scintillation light then gets transported through the wavelength shifting fiber into photomultiplier tubes where the signal is read out. The HEC is based on the same LAr technology used in the EM calorimeters, but uses copper, instead of lead, for the absorber material. Total interaction lengths of the ATLAS calorimeter system as a function of pseudorapidity are summarized in Fig. **??**. Both TileCal and HEC calorimeters have an energy resolution of $\sigma(E_T)/E_T = 50\%/\sqrt{E_T} \bigoplus 3\%$.

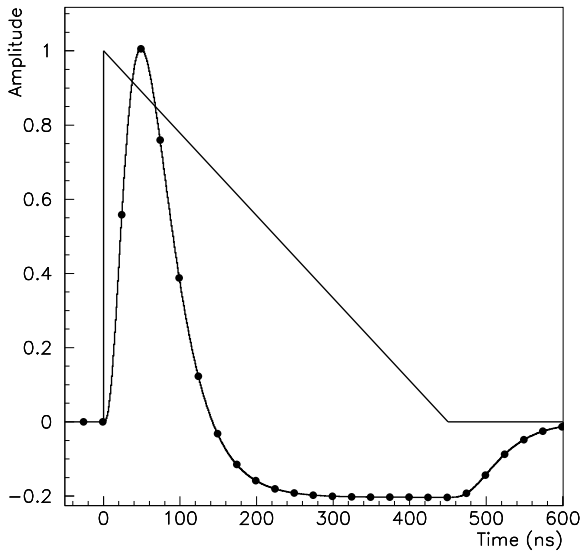

Figure 2.11: Amplitude versus time plot of a LAr calorimeter pulse before shaping (triangular). The shaped pulse is sampled every 25 ns, as indicated by the periodic points. The sampling frequency corresponds to the LHC bunch crossing frequency of 25 ns. Figure taken from Ref. [3].

Tile Barrel and Extended Barrel Calorimeters

The Tile barrel and extended barrel calorimeters cover $|\eta| < 0.8$ and $0.8 < |\eta| < 1.7$ respectively. The tile barrel calorimeter is 5.8 m long, the two tile extended barrels are each 2.6 m in length. Both the tile barrel and extended barrel calorimeters have an inner and outer diameter of 2.28 m and 4.25 m, respectively. They is composed of three layers with granularity of $\Delta\eta \times \Delta\phi = 0.1 \times 0.1$ for the first two layers, and the outermost layer with granularity $\Delta\eta \times \Delta\phi = 0.2 \times 0.1$. Each barrel consists of 64 modules roughly $\Delta\phi = 0.1$ in size. A schematic showing a TileCal module is shown in Fig. **??**.

LAr Hadronic End-Cap Calorimeter

The HEC calorimter is based the LAr technology used in the EM calorimter systems. The absorber material is copper, and the active material is LAr. The HEC covers a pseudorapidity region of $1.5 < |\eta| < 3.2$. The two barrels of the HEC each contain 32 modules symmetric in azimuth, with an outer radius of 2030 mm. The first two layers of the HEC have a granularity $\Delta\eta \times \Delta\phi = 0.1 \times 0.1$, while the last layer has a courser granularity of $\Delta\eta \times \Delta\phi = 0.2 \times 0.2$.

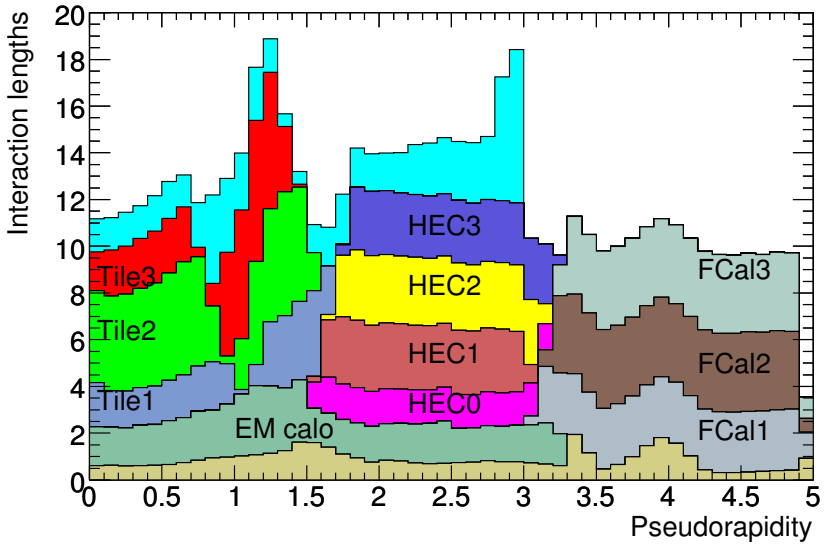

Figure 2.12: Cumulative thickness, units of interaction length (λ_I) as a function η, in front of the EM calorimeters, in the EM calorimeters themselves, in the hadronic calorimeters, and the total amount after all calorimeters. Figure taken from Ref. [3].

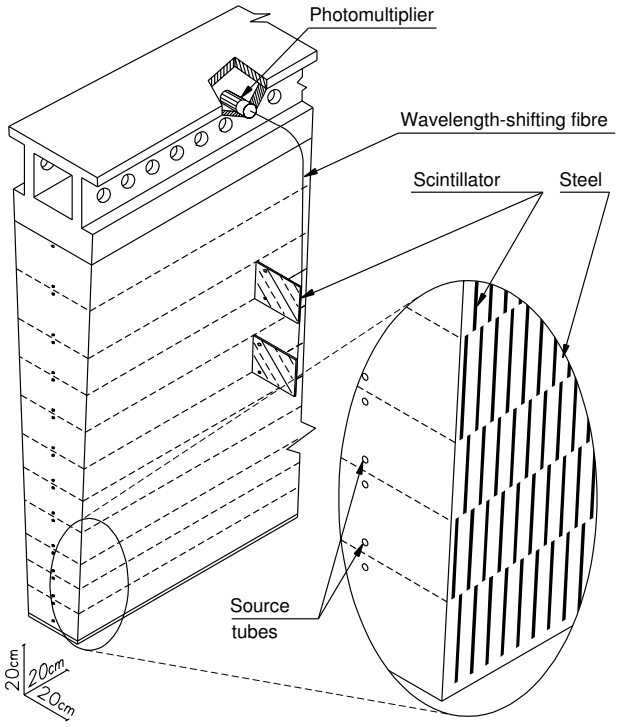

Figure 2.13: Schematic of a TileCal module, showing absorber material interspace with scintillator. Figure taken from Ref. [3].

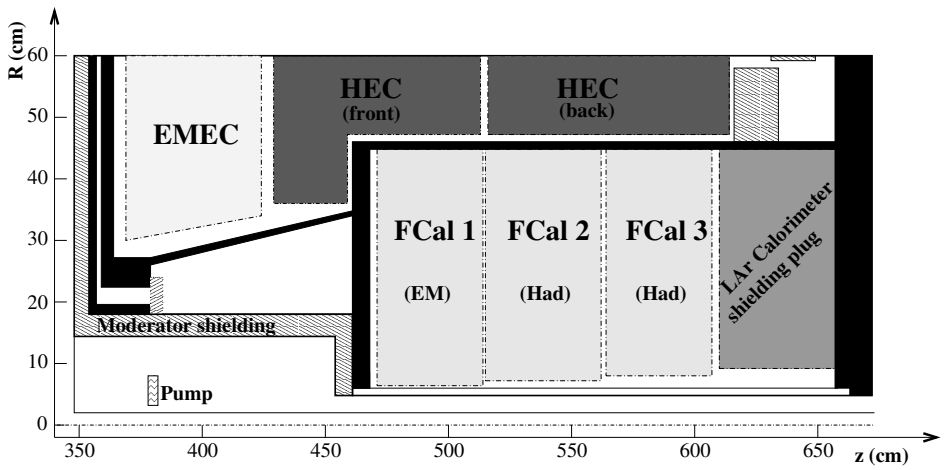

Figure 2.14: Diagram showing the three modules of the FCal. Shown in the $y - z$ plane, with the beam going in the z direction. The FCal is the most forward calorimeter in ATLAS, covering a pseudorapidity interval $3.2 < |\eta| < 4.9$. Figure taken from Ref. [3].

Forward Calorimeter

The forward calorimeter is an important sub-system in the present analysis due to its forward pseudorapidity coverage. The calorimeter is comprised of two halves located on either side of the ATLAS detector IP, surrounded by the HEC. It covers a pseudorapidity range of $3.2 < |\eta| < 4.9$, and has a granularity of $\Delta\eta \times \Delta\phi = 0.2 \times 0.2$. While the other EM calorimeter systems use an accordion design, the forward calorimeter has electrodes oriented parallel to the beamline (z-axis) which consist of thin tubes of copper with a gap for LAr that surround rods of absorber material. These tubes are located inside the same kind of absorber material. The LAr gap is thin, about 0.25 mm in the first module, in order to increase readout time and decrease noise from ion buildup.

Each FCal is composed of three modules, as shown in the $y - z$ plane in Fig. **??**. The first of three modules (FCal1) is the EM module and uses copper as the absorber. The last two hadronic modules (FCal2, FCal3) use tungsten as the absorber. FCal1 uses copper plates that are stacked one behind the other. These plates have 12,260 drilled holes to make space for the electrodes, which are rods made from absorber material coaxial to a thin surrounding LAr layer with precision, radiation-hard plastic fiber used for readout. A schematic of first layer of the calorimeter as it appears in the $x - y$ plane, perpendicular to the beam direction, showing the tubes of LAr inside the absorber material, is shown in the left of Fig. **??**. Signal is read out from ionized charges in the LAr that travel to electrodes which run parallel to the tubes. The hadronic modules FCal2 and FCal3 require large interaction lengths, which is why tungsten is chosen as the absorber material, rather than copper as in FCal1. The modules consist of two copper plates, 2.35 cm thick, that have many tungsten rods, coaxial to copper tubes with a LAr gap, enclosed in tungsten slugs, as

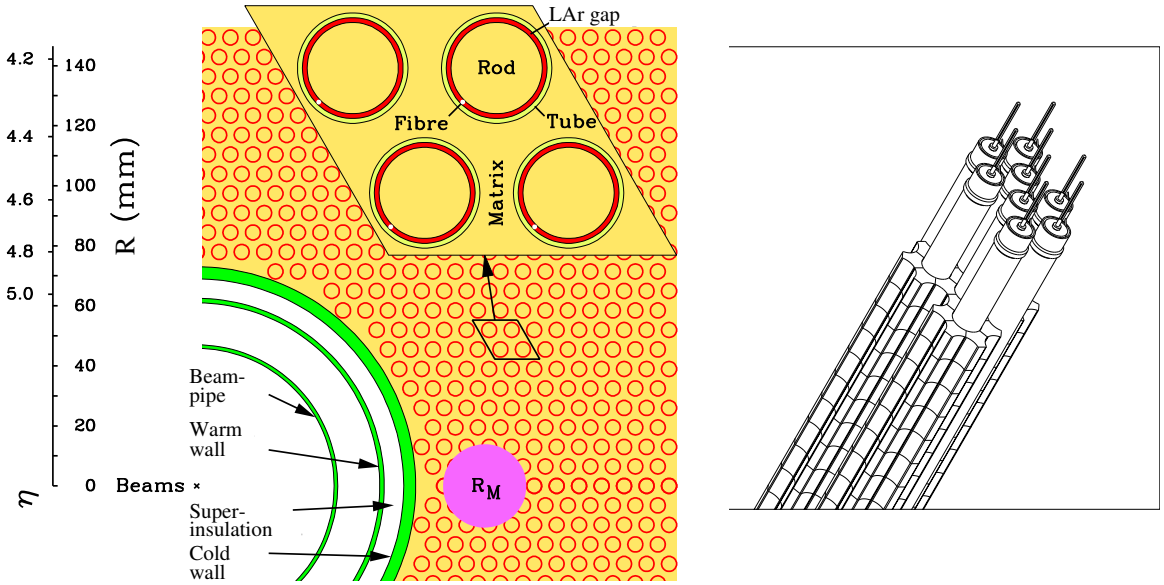

Figure 2.15: View of first FCal module (EM) as seen along the z-axis (left). Tubes of LAr inside absorber material. Shown is one Moliere radius R_M, which is the radius of a cylinder that would contain 90% of the radiation inside a calorimeter. A schematic of the tungsten rods, enclosed in copper and a LAr gap, all surrounded by tungsten slugs (right). The design is used for the two hadronic FCal modules FCal2 and FCal3. Figures taken from Ref. [3].

shown in right of Fig. **??**. These modules give a total of 10 λ_I interaction lengths. The FCal has an energy resolution of $\sigma(E_T)/E_T = 100\%/\sqrt{E_T} \bigoplus 10\%$.

2.2.3 Solenoid Magnet

The magnet system, shown in Figure **??** has an overall dimension of 22 m in dameter and 26 m in length. It stores a total energy of 1.6 GJ and consists of a barrel solenid magnet, and toroidal magnets used by the muon system. The toroidal magnets are not used in the present analysis. The solenoid magnet, which is used by the inner detector tracker, provides a 2 T axial field which is supplied by a 7.73 kA current. NbTi is used as a conductor and is supercooled by a LAr cryostat temperatures down to 4.5 K.

2.2.4 Inner Detector

The ATLAS Inner Detector (ID) is responsible for tracking, which is the precise determination of the position of charged particles. In an average collision there can be thousands of particles, which, in in the presence of a magnetic field, will curve. If their positions are well known and can be distinguished, the particles momentum can be calculated. The ID is designed to provide precision tracking for particles above a p_{T} threshold of 0.5 GeV, although some studies have had similar performance with particle p_{T} as low as 0.1

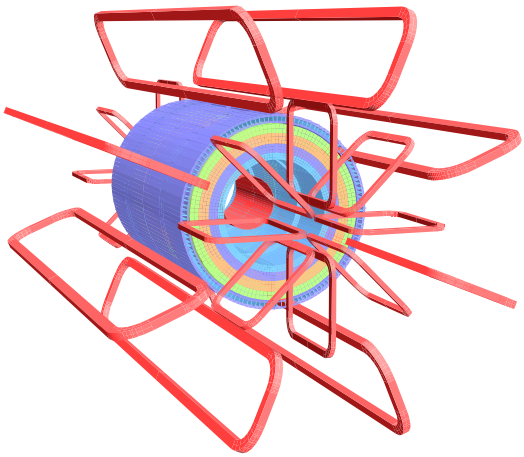

Figure 2.16: The ATLAS magnet system. Shown is the cylindrical solenoid magnet, as well as the eight barrel toroid magnets used for muon detection. Figure taken from Ref. [3].

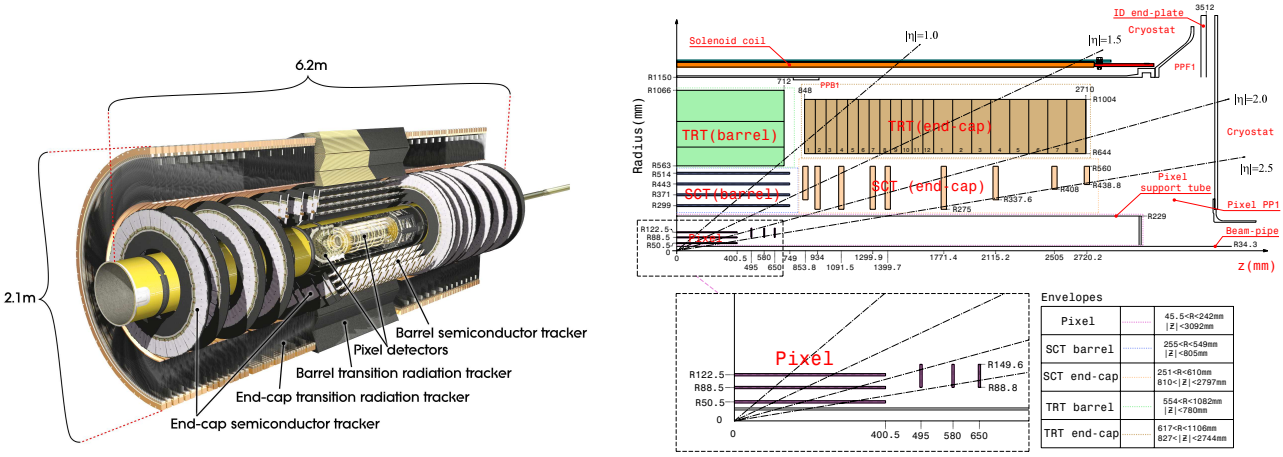

Figure 2.17: Cut-away picture (left) and schematic (right) of the ATLAS Inner Detector. Figures taken from Ref. [3].

GeV. The ID is designed to have a transverse momentum resolution of $\sigma(p_{\mathrm{T}})/p_{\mathrm{T}} = 0.05\%/\sqrt{E_T} \bigoplus 1\%$. Tracking is a very important part of every high energy particle detector, and is usually placed closest to the interaction point of a detector. A cut-away and schematic of the ID is shown in Fig. **??**. The detector sits inside the 2T magnetic field produced by the solenoid. The ID has a rapidity coverage of $|\eta| < 2.5$ and has an outer radius of 1.15 m. There are there main subsystems that comprise the ID, listed outwards from the beam pipe: the pixel detectors, the semiconductor tracker (SCT), and the transitional radiation tracker (TRT).

The pixel layer has the highest granularity out of the ATLAS tracking subsystems. There is a barrel layer and two end-cap layers, one on each side of the IP. The barrel detector has three concentric layers located 50.5mm, 88.5mm, and 122.5 mm radially away from the beam pipe. The end-caps also have three layers

located 495mm, 580mm, and 650mm in the transverse direction on each side of the interaction point. All of the pixel subsystems have a granularity of $50x400$ μm^2 and total approximately 80 million readout channels. The SCT has roughly 6.3 million channels and consists of four concentric barrel layers, and nine disks on each side of the IP. The accuracy of the barrel and end-cap regions is 17 μm in the ($R\phi$) plane and 580 μm in the radial direction. The TRT, which is a drift tube (straw) detector, is the outermost tracking layer of the ID. It has a total of approximately 351,000 channels (one per straw) and an accuracy of 130 μm per straw tube. However, during HI running, the occupancy in the TRT is usually too large to use effectively.

References

[1] G. Roland, K. Šafařík, and P. Steinberg. "Heavy-ion collisions at the LHC". In: *Prog. Part. Nucl. Phys.* 77 (2014), pp. 70–127.

[2] Wit Busza et al. "Heavy Ion Collisions: The Big Picture, and the Big Questions". In: *Ann. Rev. Nucl. Part. Sci.* 68 (2018), pp. 339–376. DOI: 10.1146/annurev-nucl-101917-020852. arXiv: 1802.04801 [hep-ph].

[3] ATLAS Collaboration. "The ATLAS Experiment at the CERN Large Hadron Collider". In: *JINST* 3 (2008), S08003.